Proceedings of the 28th IEEE
EMBS Annual International Conference
New York City, USA, Aug 30-Sept 3, 2006



# Tumor detection using Bayesian conjugate prior in diffuse optical tomography

Heeralal Choudhary and Arye Nehorai

*Abstract*— **Diffuse optical tomography (DOT) is an emerging non-invasive technique for detecting the presence of a tumor or other anomalies from a scattered photon field. In this paper, we derive an alternating projection algorithm to reconstruct the spatially varying absorption coefficient of human brain tissue to detect the presence of tumor. We use a perturbation method and assume the absorption coefficient of the tumor to be spatially varying with a Gaussian distribution. This assumption serves as a Bayesian conjugate prior on the absorption coefficient of the whole domain and using this prior can reduce the computational complexity and allow finding analytically tractable posteriors. Such prior information can be extracted from MRI or X-ray images to improve spatial resolution and accuracy of the reconstructed image. We illustrate our results using a simulated 3D geometry. We show that tumor presence can be detected using only one observation of the noisy data.**

## I. INTRODUCTION

In the recent years, diffuse optical tomography (DOT) has been proposed and studied as a potential diagnostic tool for detecting tumor growth in soft human tissue [1], [2], [3]. It is non-invasive, non-ionizing, and low cost; and thus it has attracted the attention of researchers from different areas. The forward model in DOT describes the photon propagation in human tissue and relates the optical properties of a tissue to the measurements. The inverse problem is to reconstruct the spatially varying absorption and scattering coefficients of human tissues. This problem is typically ill-posed because of the large number of unknown parameters involved [2], [3], [5]. Solutions to the inverse problem have been extensively studied [4], [11]. Researchers have used a Bayesian approach, penalty functions, and different regularization terms to incorporate *a priori* information in solving the inverse problem [7], [8], [9].

In this paper, we provide a general framework to incorporate *a priori* information using a Bayesian conjugate prior. The fundamental advantage of a conjugate prior density is to provide very easily the related posterior distribution because both densities belong to the same family of distributions. For example, in the exponential family the posterior mean is a weighted average of the prior mean and the data for the univariate case. This is possible because the distributions of data, prior, and the posterior are all Gaussian and belong to the same family, exponential family of distributions. This framework can be used with or without other modalities to solve the inverse problem. For the forward model, we use the Green function to develop the relationship between the incident and scattered photon fields, and we take care of the boundary effects using the method of images. More detailed development is given in our previous work [1]. Using the perturbation approach and Rytov approximation [4], [5], we show that the image can be reconstructed with a single noisy observation. For the inverse problem, we assume a Gaussian conjugate prior on the absorption coefficient. A zero prior mean represents the no tumor condition, which helps in developing the alternating projection algorithm with the help of data to reconstruct the image for tumor detection. Based on other modalities such as magnetic resonance imaging (MRI) or X-ray, this prior model can be modified. We show the simulation results using a spherical tumor to simplify the analysis.

The rest of the paper is organized as follows. In Section II, we describe the forward model used in this study. In Section III, we derive the inverse model using the alternating projection algorithm with a Bayesian prior on the absorption coefficient. Section IV consists of numerical examples, and Section V concludes the paper.

## II. FORWARD MODEL

In this section, we briefly review the forward model used for DOT; for a detailed description see [1], [4], [11]. We present a linear model between measurements and unknown parameters using domain decomposition.

Photon migration in soft human tissue can be modeled using the diffusion approximation (DA) of the Boltzmann transport equation [1], [4], [11] as follows:

$$\begin{aligned} \frac{\partial U(\boldsymbol{r},t)}{\partial t} + v\mu_{\mathrm{a}} U(\boldsymbol{r},t) + \nabla \cdot \boldsymbol{J}(\boldsymbol{r},t) &= q_{\mathrm{o}}(\boldsymbol{r},t), \\ \nabla U(\boldsymbol{r},t) + \frac{3\partial \boldsymbol{J}(\boldsymbol{r},t)}{v^2 \partial t} + \frac{\boldsymbol{J}(\boldsymbol{r},t)}{D} &= 0, \end{aligned} \tag{1}$$

where $U$ and $\boldsymbol{J}$ represent the photon density and photon current density, respectively; $q_{\mathrm{o}}$ is the isotropic source term and $v$ refers to the speed of light in the medium; $D\left(=\frac{v}{3\mu_{\mathrm{s}}'}\right)$ is the diffusion coefficient, assumed to be constant over the domain; $\mu_{\mathrm{a}}$ and $\mu_{\mathrm{s}}'$ are the absorption and reduced scattering coefficient of the medium, respectively. In this work, we focus on the reconstruction of the absorption coefficient of the medium. Hence, we assume only $\mu_{\mathrm{a}}$ is varying over the space. Using the Rytov approximation, the heterogenous photon density can be written as [6]

$$U(\boldsymbol{r}_{\mathrm{s}}, \boldsymbol{r}) = U_{\mathrm{o}}(\boldsymbol{r}_{\mathrm{s}}, \boldsymbol{r}) e^{\Phi_{\mathrm{sc}}(\boldsymbol{r}_{\mathrm{s}}, \boldsymbol{r})},$$

This work was supported by the National Science Foundation Grant CCR-0330342.

H. C. and A. N. are with the department of Electrical and Systems Engineering at the Washington University in St. Louis, MO 63130, USA. nehorai@ese.wustl.edu

| | |
|---|---|
| Helmholtz equation | $(\nabla^2 + k^2)U(\boldsymbol{r}) = -f(\boldsymbol{r})$ |
| Green function | $G(\boldsymbol{r}) = \frac{1}{4\pi\|\boldsymbol{r}\|}e^{jk\|\boldsymbol{r}\|}$ |
| Solution | $U(\boldsymbol{r}) = \int_\Omega G(\boldsymbol{r}, \boldsymbol{r}')f(\boldsymbol{r}')d\boldsymbol{r}'$ |

TABLE I

SOLUTION OF HELMHOLTZ EQUATION USING GREEN FUNCTION.

where $U_{\mathrm{o}}(\boldsymbol{r}_{\mathrm{s}}, \boldsymbol{r})$ is the homogenous photon density and $\Phi_{\mathrm{sc}}(\boldsymbol{r}_{\mathrm{s}}, \boldsymbol{r})$ represents the diffuse Rytov phase. Using a perturbation approach, the solution for $\Phi_{\mathrm{sc}}(\boldsymbol{r}_{\mathrm{s}}, \boldsymbol{r})$ at a specific detector location $\boldsymbol{r}_{\mathrm{d}}$ due to a source at $\boldsymbol{r}_{\mathrm{s}}$ is given by [2], [4], [11],

$$\Phi_{\mathrm{sc}}(\boldsymbol{r}_{\mathrm{s}}, \boldsymbol{r}_{\mathrm{d}}) = -\frac{3\mu_{\mathrm{s}}^{'}}{U_{\mathrm{o}}(\boldsymbol{r}_{\mathrm{s}}, \boldsymbol{r}_{\mathrm{d}})}\int_\Omega U_{\mathrm{o}}(\boldsymbol{r}_{\mathrm{s}}, \boldsymbol{r})\delta\mu_{\mathrm{a}}(\boldsymbol{r})G(\boldsymbol{r}, \boldsymbol{r}_{\mathrm{d}})d\boldsymbol{r}, \tag{2}$$

where $G$ is the Green function shown in Table I. Here $\delta\mu_{\mathrm{a}}(\boldsymbol{r})$ is the difference in the absorption coefficient of the tissue at location $\boldsymbol{r}$ w.r.t. the background. Equation (2) represents the linear relationship between the measurements and the unknowns. Discretizing the total domain $\Omega$ into $N$ equivolume voxels, we get the following relationship between the $i^{th}$ source and the $k^{th}$ detector,

$$\Phi_{\mathrm{sc}}(\boldsymbol{r}_{\mathrm{s_i}}, \boldsymbol{r}_{\mathrm{d_k}}) = -\sum_{j=1}^{N}\frac{3\mu_{\mathrm{s}}^{'}U_{\mathrm{o}}(\boldsymbol{r}_{\mathrm{s_i}}, \boldsymbol{r}_{\mathrm{j}})\delta\mu_{\mathrm{a}}(\boldsymbol{r}_j)G(\boldsymbol{r}_{\mathrm{j}} - \boldsymbol{r}_{\mathrm{d_k}})h^3}{U_{\mathrm{o}}(\boldsymbol{r}_{\mathrm{s_i}}, \boldsymbol{r}_{\mathrm{d_k}})}, \tag{3}$$

where $h^3$ represents the volume of an individual voxel. Assuming P sources and Q detectors, we write Equation (3) in matrix form,

$$\begin{bmatrix} \Phi_{\mathrm{sc}}(\boldsymbol{r}_{\mathrm{s_1}}, \boldsymbol{r}_{\mathrm{d_1}}) \\ \vdots \\ \Phi_{\mathrm{sc}}(\boldsymbol{r}_{\mathrm{s_i}}, \boldsymbol{r}_{\mathrm{d_k}}) \\ \vdots \\ \Phi_{\mathrm{sc}}(\boldsymbol{r}_{\mathrm{s_P}}, \boldsymbol{r}_{\mathrm{d_Q}}) \end{bmatrix} = \begin{bmatrix} W_{111} & \cdots & W_{11\mathrm{N}} \\ \vdots & \ddots & \vdots \\ W_{\mathrm{ik1}} & \cdots & W_{\mathrm{ikN}} \\ \vdots & \ddots & \vdots \\ W_{\mathrm{PQ1}} & \cdots & W_{\mathrm{PQN}} \end{bmatrix} \begin{bmatrix} \delta\mu_{\mathrm{a}}(\boldsymbol{r}_1) \\ \vdots \\ \delta\mu_{\mathrm{a}}(\boldsymbol{r}_j) \\ \vdots \\ \delta\mu_{\mathrm{a}}(\boldsymbol{r}_N) \end{bmatrix}, \tag{4}$$

where $W_{\mathrm{ikj}}$ represents the effects of the $i^{th}$ source on the $j^{th}$ voxel measured at the $k^{th}$ detector and is given by

$$W_{\mathrm{ikj}} = -\frac{3\mu_{\mathrm{s}}^{'}U_{\mathrm{o}}(\boldsymbol{r}_{\mathrm{s_i}}, \boldsymbol{r}_{\mathrm{j}})G(\boldsymbol{r}_{\mathrm{j}} - \boldsymbol{r}_{\mathrm{d_k}})h^3}{U_{\mathrm{o}}(\boldsymbol{r}_{\mathrm{s_i}}, \boldsymbol{r}_{\mathrm{d_k}})}.$$

We rewrite Equation (4) in a short form as

$$\boldsymbol{\Phi}^c = \boldsymbol{W}^c\boldsymbol{\Delta}, \tag{5}$$

where $\boldsymbol{\Phi}^c$ is the complex measurement vector, $\boldsymbol{W}^c$ the complex weight matrix, and $\boldsymbol{\Delta}$ the vector of unknown changes in the absorption coefficients of voxels.

## III. INVERSE PROBLEM AND CONJUGATE PRIOR

In this section, we describe the method used to solve the inverse problem using a Bayesian conjugate prior. Before starting the mathematical model for the inverse problem, we state one theorem and the assumptions about the noise.

We assume that all the measurements are corrupted by shot noise. Shot noise is caused by the randomness in photon arrival time at the detector. It follows poisson statistics, which can be approximated as a Gaussian random variable if the number of photons arriving at the detector is very large. Since the variance of shot noise is expected to be proportional to the number of photons arriving at the detector during a given time interval, it can be modeled as a multiplication of signal intensity and a random variable. Hence, our measurement model is given by:

$$\boldsymbol{\Phi}^c = \boldsymbol{W}^c\boldsymbol{\Delta} + \boldsymbol{\xi}^c, \tag{6}$$

where $\boldsymbol{\xi}^c$ follows a complex Gaussian distribution with zero mean and covariance matrix $\boldsymbol{\Sigma}$, i.e. $\boldsymbol{\xi}^c \sim \mathcal{CN}(0, \boldsymbol{\Sigma})$. The covariance matrix $\boldsymbol{\Sigma}$ can be written as,

$$\boldsymbol{\Sigma} = \begin{bmatrix} \lambda|\boldsymbol{\Phi}_{11}^c| & \cdots & 0 \\ \vdots & \ddots & \vdots \\ 0 & \cdots & \lambda|\boldsymbol{\Phi}_{PQ}^c| \end{bmatrix} = \lambda\boldsymbol{\Sigma}_\Phi, \tag{7}$$

where $\boldsymbol{\Phi}_{ij}^c$ represents the complex measurement at the $j^{th}$ detector due to the $i^{th}$ source. For convenience, we write the complex matrix Equation (6) in the following form:

$$\begin{bmatrix} \Re\boldsymbol{\Phi}^c \\ \Im\boldsymbol{\Phi}^c \end{bmatrix} = \begin{bmatrix} \Re\boldsymbol{W}^c \\ \Im\boldsymbol{W}^c \end{bmatrix}\boldsymbol{\Delta} + \begin{bmatrix} \Re\boldsymbol{\xi}^c \\ \Im\boldsymbol{\xi}^c \end{bmatrix}, \tag{8}$$

where the operators $\Re(\cdot)$ and $\Im(\cdot)$ take the real and imaginary parts of a complex vector respectively. Hence, in the real domain we define $\boldsymbol{\Phi} = \begin{bmatrix} \Re\boldsymbol{\Phi}^c \\ \Im\boldsymbol{\Phi}^c \end{bmatrix}$, $\boldsymbol{W} = \begin{bmatrix} \Re\boldsymbol{W}^c \\ \Im\boldsymbol{W}^c \end{bmatrix}$, $\boldsymbol{\xi} = \begin{bmatrix} \Re\boldsymbol{\xi} \\ \Im\boldsymbol{\xi} \end{bmatrix}$, and obtain the following linear model:

$$\boldsymbol{\Phi} = \boldsymbol{W}\boldsymbol{\Delta} + \boldsymbol{\xi}, \tag{9}$$

where the noise vector $\boldsymbol{\xi}$ follows a real Gaussian distribution with zero mean and covariance matrix $\widetilde{\boldsymbol{\Sigma}}$ and where

$$\widetilde{\boldsymbol{\Sigma}} = \frac{\lambda}{2}\begin{bmatrix} \boldsymbol{\Sigma}_\Phi & 0 \\ 0 & \boldsymbol{\Sigma}_\Phi \end{bmatrix} = \frac{\lambda}{2}\boldsymbol{\Xi}. \tag{10}$$

Based on the above derivation, the probability density function of the random variable $\boldsymbol{\Phi}$ can be written as,

$$p(\boldsymbol{\Phi}, \lambda|\boldsymbol{\Delta}) = \frac{1}{(2\pi\lambda)^K|\boldsymbol{\Xi}|^{1/2}}e^{-\frac{1}{\lambda}(\boldsymbol{\Phi}-\boldsymbol{W}\boldsymbol{\Delta})'\boldsymbol{\Xi}^{-1}(\boldsymbol{\Phi}-\boldsymbol{W}\boldsymbol{\Delta})}, \tag{11}$$

where we define $K = PQ$.

We propose a Bayesian approach to reconstruct the unknown parameter vector $\boldsymbol{\Delta}$. In particular, this prior information can be derived from any other modality like MRI or X-ray. Our prior model assumes that $\boldsymbol{\Delta}$ follows a Gaussian distribution with zero mean and covariance matrix $\boldsymbol{\Sigma}_\Delta$. The prior distribution for $\boldsymbol{\Delta}$ can be justified using the perturbation approach. Since $\boldsymbol{\Delta}$ consists of $\delta\mu_{\mathrm{a}}$, which describes the change in the

value of the absorption coefficient due to perturbation and inhomogeneity, we expect the mean value to be zero for each voxel. In the physical realm, it indicates that there is no tumor in the domain. Also, the covariance of $\boldsymbol{\Delta}$, $\boldsymbol{\Sigma}_\Delta$, is related to the type of inhomogeneity or the effect of perturbation (in the homogenous part). Since we do not expect the perturbation to change the absorption properties significantly as compared to the added inhomogeneity, we should have a large variance for inhomogeneity as compared to the homogenous part. Also, changes in the absorption properties of inhomogeneity should not be affected by changes in the absorption properties of the homogenous part; hence we expect cross correlation to be zero. Within the homogenous part or the inhomogeneous part, we can expect a non-zero cross correlation only between neighboring voxels. Hence, the general nature of $\boldsymbol{\Sigma}_\Delta$ is block diagonal, but for simplicity of analysis, we assume $\boldsymbol{\Sigma}_\Delta$ to be diagonal.

Based on this prior distribution, the joint distribution can be written as

$$\begin{aligned} p(\boldsymbol{\Phi},\lambda,\boldsymbol{\Delta}) &= p(\boldsymbol{\Phi},\lambda|\boldsymbol{\Delta})p(\boldsymbol{\Delta}) \\ &= \frac{1}{(2\pi)^{\frac{2K+1}{2}}\lambda^K|\boldsymbol{\Xi}|^{1/2}|\boldsymbol{\Sigma}_\Delta|^{1/2}}\cdot \\ &\quad e^{-\frac{1}{\lambda}(\boldsymbol{\Phi}-\boldsymbol{W}\boldsymbol{\Delta})'\boldsymbol{\Xi}^{-1}(\boldsymbol{\Phi}-\boldsymbol{W}\boldsymbol{\Delta})}\cdot \\ &\quad e^{-\frac{1}{2}\boldsymbol{\Delta}'{\boldsymbol{\Sigma}_\Delta}^{-1}\boldsymbol{\Delta}}. \end{aligned} \tag{12}$$

To obtain the optimal solutions for $\lambda$ and $\Delta$, we use a recursive alternating projection algorithm. We initialize the algorithm with any nonzero value of $\lambda$. For any particular $\lambda = \widehat{\lambda}$, $\Delta$ and the error covariance matrix can be written using a Bayesian conjugate prior for an unknown mean and known covariance matrix as in [10]:

$$\begin{aligned} \widehat{\Delta} &= E[\Delta|\boldsymbol{\Phi}=\Phi] \\ &= \boldsymbol{\Sigma}_\Delta \boldsymbol{W}'\left(\boldsymbol{W}\boldsymbol{\Sigma}_\Delta\boldsymbol{W}'+\frac{\widehat{\lambda}}{2}\boldsymbol{\Xi}\right)^{-1}\Phi, \end{aligned} \tag{13}$$

$$\begin{aligned} \text{BMMSE} &= V[\Delta|\boldsymbol{\Phi}=\Phi] \\ &= \boldsymbol{\Sigma}_\Delta - \boldsymbol{\Sigma}_\Delta\boldsymbol{W}'\left(\boldsymbol{W}\boldsymbol{\Sigma}_\Delta\boldsymbol{W}'+\frac{\widehat{\lambda}}{2}\boldsymbol{\Xi}\right)^{-1}\boldsymbol{W}\boldsymbol{\Sigma}_\Delta. \end{aligned}$$

Here BMMSE stands for Bayesian minimum mean square error and is given by the covariance matrix of the *posteriori* distribution. We define a mean error measurement to evaluate the performance of our model:-mean Bayesian minimum mean square error (MBMMSE):

$$\text{MBMMSE} = \mathbf{1}'V[\Delta|\boldsymbol{\Phi}=\Phi]\mathbf{1}/K, \tag{14}$$

where $\mathbf{1}$ is a $N \times 1$ vector of all ones. We observe that the estimation of the unknown variable $\Delta$ is a weighted average between the data and the prior mean. Hence while initially the estimation may be more inclined towards the prior mean, as soon as we know the data measurements, our estimation starts incorporating the information extracted from the data model. Thus the success of this model also depends on the accuracy of the prior model. In the case of a noninformative prior (for example, a uniform prior), the model is equivalent to the non-Bayesian case. Once we estimate $\widehat{\Delta}$, the maximum likelihood estimation (MLE) of $\lambda$ can be obtained by differentiating the joint distribution $p(\boldsymbol{\Phi},\lambda,\boldsymbol{\Delta})$ w.r.t. $\lambda$, which yields

$$\widehat{\lambda} = \frac{1}{K}\left(\boldsymbol{\Phi}-\boldsymbol{W}\widehat{\Delta}\right)'\boldsymbol{\Xi}^{-1}\left(\boldsymbol{\Phi}-\boldsymbol{W}\widehat{\Delta}\right). \tag{15}$$

Now we recursively compute $\widehat{\Delta}$ and $\widehat{\lambda}$ till we reach a convergence. We define convergence as having occurred when the new estimate $\widehat{\lambda}$ is negligibly different from the old estimates, i.e. $|\widehat{\lambda}_{\text{new}} - \widehat{\lambda}_{\text{old}}| < \epsilon$ where $\epsilon$ is a small number.

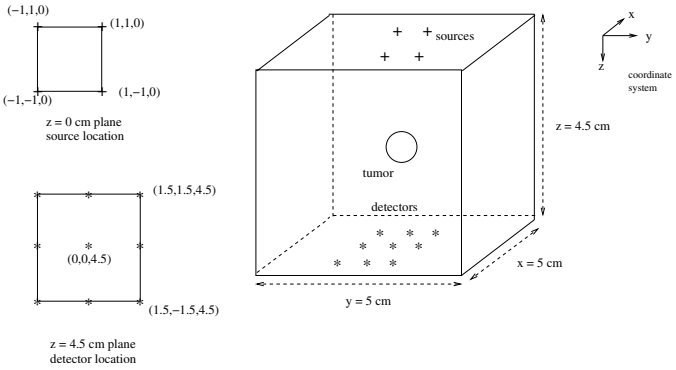


Fig. 1. The system setup used for the simulation of alternating projection algorithm. Sources and detectors are shown at the top and bottom surfaces, respectively. The origin of the coordinate system lies at the center of the top surface $z = 0$.

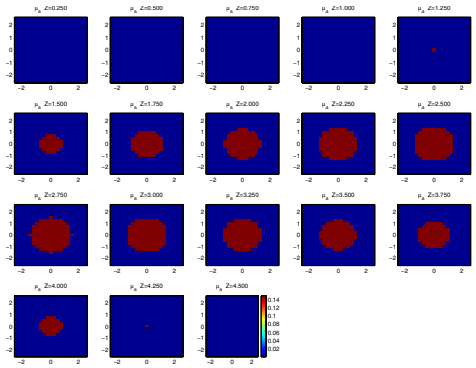

Fig. 2. The original image used for the simulation. Here we show the sliced version of the previous figure. Different small images show the cross section layers at different $z$ values with a constant difference of 0.25 cm between different layers.

## IV. NUMERICAL EXAMPLES

In this section, we illustrate the performance of our model through a simulated geometry shown in Fig. 1. We used a cuboidal geometry of size $5 \times 5 \times 4.5$ cm$^3$. The origin of the coordinate system is at the center of the top surface, with the directions of the coordinate axes shown in the figure. The $x, y$, and $z$ coordinate range are $[-2.5, 2.5]$ cm, $[-2.5, 2.5]$ cm, and $[0, 4.5]$ cm, respectively. We placed four sources on the top surface represented by $z = 0$ and nine detectors on the bottom surface $z = 4.5$ cm, resulting in

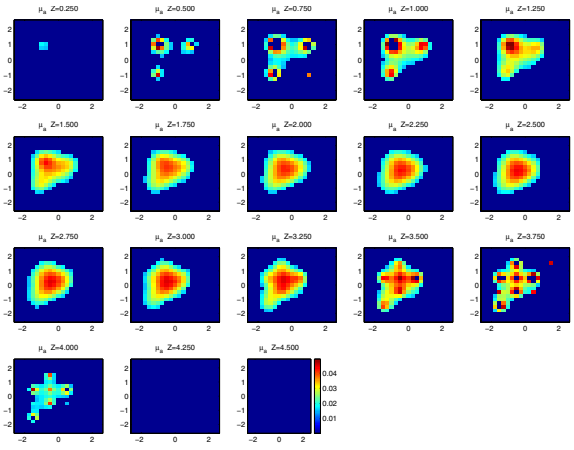

Fig. 3. The reconstructed image using measurements at a single wavelength.

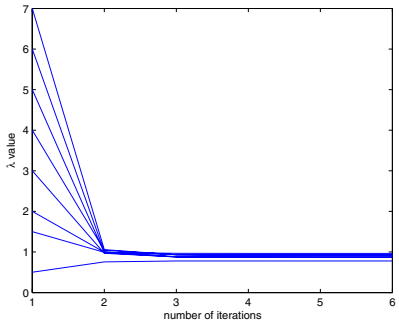


Fig. 4. The convergence of the $\lambda$ value for different sets of initial values. For details, refer to Table II.

a total of 36 measurements. We placed a spherical tumor of radius 1.5 cm and absorption coefficient of 0.55 $\text{cm}^{-1}$ at $(0, 0, 2.75)$ cm. We used an absorption coefficient of 0.4 $\text{cm}^{-1}$, a reduced scattering coefficient of 15 $\text{cm}^{-1}$, and a fixed $g = 0.9$. The refractive index of the geometry was 1.37. The wavelength of the light used was 800 nm. The domain was discretized into uniform voxels, where each voxel volume was $0.25 \times 0.25 \times 0.25$ $\text{cm}^3$. To measure the scattered photon flux we used the Rytov approximation described in the Section II. To incorporate the *a priori* information about the unknown changes in the absorption coefficient we assumed a multivariate Gaussian model with zero mean and covariance matrix as a diagonal matrix of the value 0.4 for each voxel, i.e. $\mathbf{\Sigma}_\Delta = (\sigma_{\text{ij}})$ with $\sigma_{\text{ii}} = 0.4 \forall i = j$ and $\sigma_{\text{ij}} = 0 \forall i \neq j$.

The original image and the reconstructed image are shown in Fig. 2 and Fig. 3, respectively. We assumed a shot noise model with parameter $\lambda = 1$. The reconstruction is based on a single noisy observation at a single frequency. We initialized the algorithm with an arbitrary value of $\lambda$. For this particular reconstruction, we chose $\lambda = 9$ as the initial guess. The algorithm converges within 5 iterations. Fig. 4 and Table II show the convergence of the algorithm for $\lambda$ with different initial values.

| | | | | | |
|---|---|---|---|---|---|
| 0.5 | 0.7563 | 0.7773 | 0.7788 | 0.7788 | 0.7788 |
| 1.5 | 0.9928 | 0.9666 | 0.9649 | 0.9648 | 0.9648 |
| 2 | 0.9935 | 0.9348 | 0.9302 | 0.9298 | 0.9298 |
| 3 | 0.9671 | 0.8770 | 0.8694 | 0.8688 | 0.8687 |
| 4 | 1.0408 | 0.9307 | 0.9213 | 0.9204 | 0.9204 |
| 5 | 0.9797 | 0.8754 | 0.8688 | 0.8684 | 0.8683 |
| 6 | 0.9999 | 0.8859 | 0.8772 | 0.8765 | 0.8764 |
| 7 | 1.0579 | 0.9314 | 0.9225 | 0.9218 | 0.9218 |

TABLE II

This table shows the convergence for $\lambda$. The first column represents the initial value used for the simulation. Second and the later columns represent the values obtained for $\lambda$ after the first, second, third, fourth, and fifth iterations.

## V. CONCLUSION AND FUTURE WORK

Our analysis shows the preliminary results of the Bayesian conjugate prior method on a simulated geometry. This prior has resulted in a simple and interpretable solution. By analysis and numerical simulations, we have shown that the tumor can be detected even using a single observation. Our future research direction is based on the extension of this algorithm to multiple wavelengths with real images. We plan to use actual anatomical images, which will be more helpful in the tumor detection problem using DOT.

## REFERENCES


[1] H. Choudhary and A. Nehorai, "Validity bounds for tumor detection and estimation using Born approximation in diffuse optical tomography," submitted to the journal *Physics in Medicine and Biology*, Feb. 2006.

[2] S. R. Arridge, "Optical tomography in medical imaging," *Inverse Problems*, vol. 15, pp. 41-93, 1999.

[3] D. A. Boas, D. H. Brooks, E. C. Miller, C. A. DiMarzio, M. Kilmer, R. J. Gaudette, and Q. Zhang, "Imaging the body with diffuse optical tomography," *IEEE Signal Processing Magazine*, vol. 18, no. 6, pp. 57-75, Nov. 2001.

[4] J. B. Fishkin and E. Gratton, "Propagation of photon-density waves in strongly scattering media containing an absorbing semi-infinite plane bounded by a straight edge," *Journal of the Optical Society of America,* vol. 10, no. 1, pp. 127-140, Jan. 1993.

[5] M. Guven, B. Yazici, X. Intes, and B. Chance, "Diffuse optical tomography with a priori anatomical information," *Proc. SPIE Optical Tomography and Spectroscopy of Tissue*, vol. 5138, pp. 268-280, 2003.

[6] M. Guven, B. Yazici, X. Intes, B. Chance, and Y. Zheng, "Recursive least square algorithm for optical diffuse tomography," *Proceedings of the IEEE 28th Annual Northeast Bioengineering conference*, vol. 2, pp. 273-274, 2002.

[7] A. H. Hielscher and S. Bartel, "Use of penalty terms in gradient-based iterative reconstruction schemes for optical tomography," *Journal of Biomedical Optics*, vol. 6, no. 2, pp. 183-192, 2001.

[8] S. Oh, A. B. Milstein, R. P. Millane, C. A. Bouman, and K. J. Webb, "Source-detector calibration in three dimensional diffuse optical tomography," *Journal of the Optical Society of America,* vol. 19, pp. 1983-1993, 2002.

[9] B. W. Pogue, T. O. McBride, J. Prewitt, U. L. Osterberg, and K. D. Paulsen, "Spatially varying regularization improves diffuse optical tomography," *Applied Optics,* vol. 38, pp. 2950-2961, 1999.

[10] S. M. Kay, *Fundamentals of Statistical Signal Processing: Estimation Theory*, PTR Prentice-Hall, Inc. New Jersey, 1993.

[11] M. A. O'Leary, "Imaging with diffuse photon density waves," *PhD thesis*, University of Pennsylvania, 1996.